Journal of Applied Physics

RESEARCH ARTICLE | MARCH 01 2024

Effects of structural defects on optical properties of $In_xGa_{1-x}N$ layers and quantum wells

Special Collection: Native Defects, Impurities and the Electronic Structure of Compound Semiconductors: A Tribute to Dr. Wladyslaw Walukiewicz

Z. Liliental-Weber ; Roberto dos Reis

J. Appl. Phys. 135, 095703 (2024)
https://doi.org/10.1063/5.0185713

AIP Publishing

Journal of Applied Physics ARTICLE pubs.aip.org/aip/jap

Effects of structural defects on optical properties of $In_xGa_{1-x}N$ layers and quantum wells

Cite as: J. Appl. Phys. 135, 095703 (2024); doi: 10.1063/5.0185713
Submitted: 1 November 2023 · Accepted: 11 February 2024 ·
Published Online: 1 March 2024

Z. Liliental-Weber[1,a)] and Roberto dos Reis[2]

AFFILIATIONS

[1]Materials Science Division (affiliate), Lawrence Berkeley National Laboratory, Berkeley California 94720, USA
[2]Department of Materials Science and Engineering, Northwestern University, Evanston, Illinois 60208, USA

Note: This paper is part of the Special Topic on Native Defects, Impurities and the Electronic Structure of Compound Semiconductors: A Tribute to Dr. Wladyslaw Walukiewicz.

[a)]**Author to whom correspondence should be addressed:** zuzannalw@yahoo.com and z_liliental-weber@lbl.gov

ABSTRACT

This review concentrates on the microstructure of $In_xGa_{1-x}N$ layers and quantum wells (QWs) in relation to their optical properties. The microstructure of $In_xGa_{1-x}N$, with a constant In(x) concentration, shifts with layer thickness. Only layers below 100 nm for x = 0.1 are nearly defect-free. A photoluminescence peak is observed at 405 nm, in line with ~10% In, suggesting band-edge luminescence. Layers with greater thickness and In content present a corrugated surface with numerous structural defects, including V-defects, causing redshifts and multi-peaks in photoluminescence up to 490 nm. These defects, resembling those in GaN, lead to a corrugated sample surface. Atomic force microscopy shows a 3.7-fold larger corrugation in samples with 20 QWs compared to those with 5 QWs measured on $2 \times 2\,\mu m^2$ areas. Like in GaN, dual growth on different crystallographic planes results in varied QW thicknesses, influencing optical traits of devices made from $In_xGa_{1-x}N$ layers. The purpose of this review and the chosen subject is to highlight the significant contribution of Wladek Walukiewicz and his group to the current research on the properties of $In_xGa_{1-x}N$, which are crucial alloys in the field of optoelectronics.

I. INTRODUCTION

In recent three decades, rapid progress in the growth of GaN and its ternaries ($Al_xGa_{1-x}N$ and $In_xGa_{1-x}N$) revolutionized the application of these materials in the development of optoelectronics, photovoltaics, and power devices.[1–8] In particular, $In_xGa_{1-x}N$ provides the possibility of obtaining light emission with a wide-range of wavelengths, depending on the In content. InN is a key element in InGaN-based light emitting diodes (LEDs) and high speed electronics due to low electronic effective mass and high electron mobility. A controversy about the fundamental bandgap of InN led to a more intense study of this material. The initial measurement of a strong absorption edge for RF-sputtered polycrystalline InN with high electron concentration ($10^{19}\,cm^{-3}$) and low mobility ($100\,cm^2\,V^{-1}\,s^{-1}$) at 1.9 eV was assigned to its energy gap.[9] This value was accepted as the InN bandgap for a long time. To explain this, it was assumed that the 1.9 eV bandgap might come from the contribution from indium oxide or hydrogen related phase[10,11] since, indeed, a higher O (or H) concentration would lead to a higher electron concentration[12] observed in such polycrystalline films. However, a high concentration of O would be required since 24% of O would be needed to give an alloy with 1.7 eV bandgap, an even higher concentration of O would be required to explain the 1.9 eV bandgap. Such a concentration of O was never detected in such sputter-grown InN. To explain this high value on the InN bandgap, it was considered that some point defects such as nitrogen vacancies[10] and dislocations[13] can act as donors and can be responsible for this energy gap of InN. However, the research on GaN and their ternaries but particularly of $In_xGa_{1-x}N$ showed that the bandgap is decreasing with the higher x (In content).[14] In addition, Yamaguchi *et al.*[15] suggested that the bandgap of $In_xGa_{1-x}N$ might be explained by a large bowing parameter. The bandgap of InN was resolved with a high purity epitaxial InN layer grown by molecular beam epitaxy (MBE) with high electron mobility and electron concentration as low as $3 \times 10^{17}\,cm^{-3}$, which showed a low energy gap $E_g = 0.67 \pm 0.05$ eV.[16–22] The determination of

the small bandgap of InN was based on photoluminescence (PL) measurements, absorption spectroscopy, and photomodulated reflection (PR) measurements.[19, 21–22] This low energy gap of InN was later also supported by different theoretical calculations.[23–24] Using this low bandgap of InN, Walukiewicz *et al*[21] were able to fit the bandgap of $In_xGa_{1-x}N$ ($In_xAl_{1-x}N$) obtained by them and other researchers over the entire composition range using the bandgap bowing equation,

$$E_g^{In_xGa(Al)_{1-x}N(x)} = E_g^{Ga(Al)N}x + E_g^{InN}(1-x) - bx(1-x).$$

Bowing parameters b = 1.4 and 3 eV were obtained for InGaN and InAlN, respectively. Because of the direct band nature and a large bandgap tunability (0.7–3.4 eV), InGaN-based semiconductor alloys offer tremendous potential for solid-state lighting (SSL), full spectrum photovoltaic devices, and multicolor detectors. Since the InGaN energy gap covers a spectral range from the near infrared for InN to the near ultraviolet for GaN, this single semiconductor system can provide the key active layers for efficient lighting applications covering the full visible spectrum.[12, 21–22]

As a different In content in ternary InGaN leads to the change in the bandgap and, therefore, the wavelength of the emitting light, it is important to know how the microstructure of such layers is changing with changing composition and the layer thickness and how it correlates with the optical properties. In this brief review, we present from studies using transmission electron microscopy (TEM), x-ray diffraction (XRD), x-ray reciprocal maps, photoluminescence (PL), cathodoluminescence (CL), and Rutherford backscattering spectroscopy (RBS) on InGaN layers as well as quantum wells (QWs) with different In compositions and layer thicknesses, and correlate the structure of such samples with their optical properties: samples with the constant nominal (estimated by the grower based on their growth parameters) In content of 10% (x = 0.1), but different layer thicknesses, and samples with similar thickness but higher In contents (28% and 45%). These results will then be compared to the structures of quantum well samples, which are commonly used for many optoelectronic devices.

II. SAMPLES WITH In CONTENT OF 10%

Due to the large size difference between Ga and In atoms, the growth of the $In_xGa_{1-x}N$ has proven to be challenging, and structural defects of high density are normally present in layers with high In content and/or thick layers. In this work, we describe how the structural perfection and In distribution changes in InGaN layers with the same nominal composition (x = 10%) but different nominal thicknesses (100–1000 nm). Samples were grown by metalorganic chemical vapor deposition (MOCVD) on 0.5 μm GaN grown on Al_2O_3. The same samples were studied by transmission electron microscopy (TEM) in plan-view and cross-sectional configuration with the support of other methods mentioned above. These studies were described earlier,[25–29] but some new details concerning these studies are provided here. InGaN thickness measured from TEM calibrated micrographs was always slightly smaller than that estimated by the grower and is shown in Table I. Using the results by Walukiewicz *et al.*,[21] the composition dependent bandgap (and, therefore, the wavelength) from the In content of InGaN alloys was calculated with the b = 1.4 eV and is shown in Fig. 1. By correlating CL and PL emissions from small areas of the samples with composition, the role of possible structural defects can be evaluated.

TABLE I. TEM and RBS sample thickness estimation in comparison with the nominal values; in the bottom row, we show proposed sublayer thicknesses and In content in order to best fit the experimental Rutherford backscattering (RBS) spectra. Nominal thickness values are indicated at the bottom.

TEM	69	200	400	513	730
RBS	63	164	330	482	693
Nominal	100	250	500	750	1000

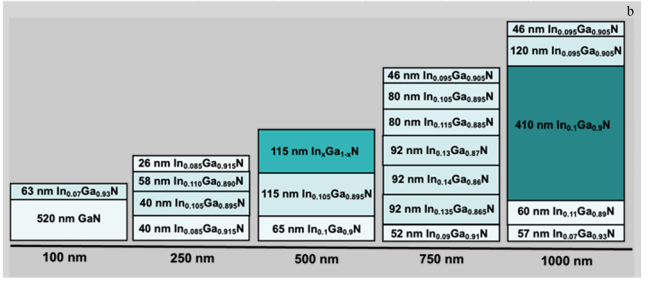

A. Structural defects

TEM studies on InGaN layers with nominal 10% In but different thicknesses showed that only the 70 nm (nominal 100 nm) thick samples had almost a flat surface (Fig. 2). There were no misfit dislocations formed at the GaN/InGaN interface. However, very shallow V-defects can be noticed where dislocations protrude the sample surface. These shallow V-defects were also noticeable in the dislocation free areas (right-hand side of Fig. 2). Generally, these thin layers were almost defect free, but occasionally stacking faults can be found. These are the most common defects in all studied InGaN samples.

Reciprocal space maps (RSMs) for the symmetrical 0002 reflections and asymmetrical $\underline{11}24$ reflection were used to determine the strain status of the layers. From the 0002 symmetrical space maps (not shown here but described earlier in Ref. 25), it was concluded that the lattice planes of the InGaN were not tilted with respect to the underlying GaN layer, and, therefore, the asymmetrical space maps give direct information about the strain state of the layers. Figure 3(a) shows the asymmetrical $\underline{11}24$ RSM for the nominally 100 nm thin InGaN layer showing that the layers are strained. A straight vertical line can connect both nodes (GaN and InGaN). The slight elongation of the InGaN node may suggest some variations in the InN composition and may be caused by the TEM observed shallow V-defects and/or the occasionally formed stacking faults. Using the layer thickness from TEM measurements (~70 nm), it was estimated that the In content in these samples was 7.3% ± 0.5% (nominally 10%).

The thicker InGaN layers with similar In composition, namely, 200, 400, 520, and 730 nm (nominally 250, 500, 750, and

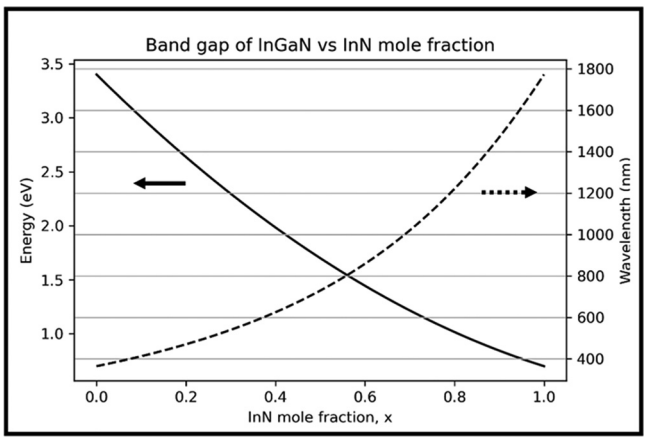

FIG. 1. The calculated energy gap and wavelength using a bowing parameter of b = 1.4 eV in dependence of InN mole fraction.

1000 nm thick, respectively) consisted of two sub-layers: a strained one and a relaxed one. A much lower In content was observed in the strained sub-layer than in the relaxed one. Based on the root mean squared (RMS) measurements, the estimated In concentration in the samples 200 nm thick (nominally 250 nm) was 7.3% ± 0.5% in a 70 nm thick strained layer, similar to that in the previous thin sample, and a 10.5% ± 0.5% in the 130 nm relaxed layer. For this sample and all thicker samples, a second node appeared on the asymmetrical RMS on an inclined line with node intensity increasing with

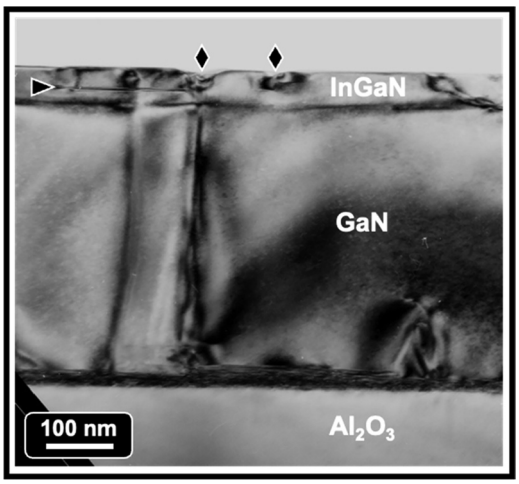

FIG. 2. InGaN strained layer with nominal 10% In and small thickness of t ~ 70 nm (nominal 100 nm) grown over GaN/Al_2O_3. No misfit dislocations formed at this interface with GaN. The layers are almost defect free, but in some areas, stacking faults are present (marked by an arrow). Note that small surface depletions at the surface in areas where dislocation protrudes the surface as well as dislocation free areas (shallow V-defects-marked by diamonds).

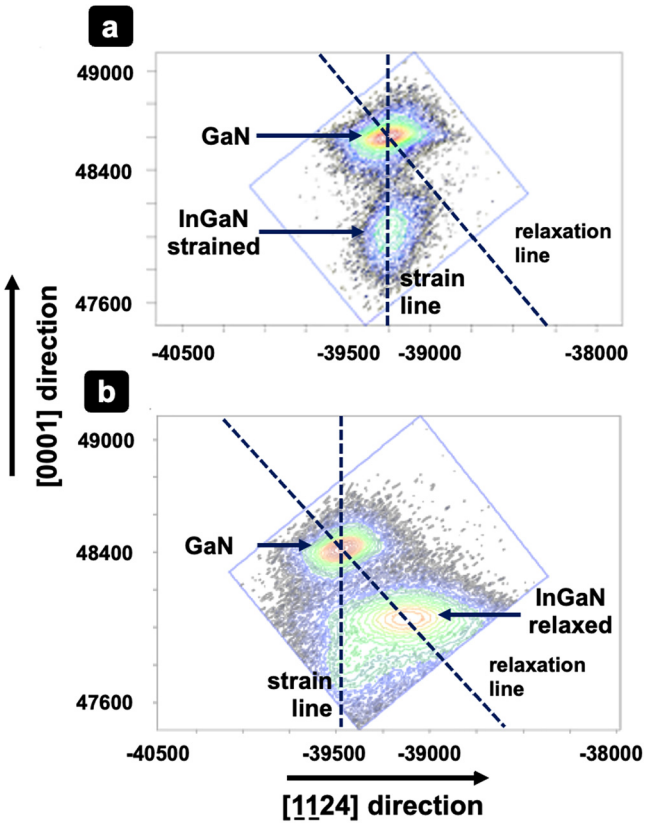

FIG. 3. (a) The reciprocal space map (RSM) for the 79 nm InGaN (nominal 100 nm) for asymmetrical 1124 reflection; (b) the RSM for the 400 nm InGaN (nominal 500 nm). Note the formation of two nodes for this sample suggesting the formation of two layers with different lattice parameters.

the sample thickness. Figure 3(b) shows an example of the 1124 asymmetrical RMS from the 400 nm thick (nominally 500 nm) InGaN, which clearly shows the presence of a second node, which suggests the formation of a relaxed layer. The estimated In composition in these layers was 7.7% ± 0.5% in the 70 nm thick strained layer and 8.1% ± 0.5% in the 330 nm thick relaxed layer. The In composition of the second layer in the thicker 520 nm thick layers (nominally 750 nm) was 7.8% ± 0.5% in the strained and 9.4% ± 0.5% in the relaxed layers. For the thickest 750 nm (nominally 1000 nm) layer, the RMS still shows two nodes with a more diffused node adjacent to the GaN, indicating~ 7.4% In and a more well-defined node for the upper part of the layer that indicates only a slightly higher In content of 7.5%. These RMS studies are further complemented with TEM results, confirming that thick InGaN layers grown on GaN do not have the same composition in the entire layer but decomposed into two sub-layers: a thin strained layer with low In (~ 7%) close to GaN and a relaxed layer with higher In content on top.

In one of our previous studies[29] on InGaN with nominal In composition 10% and a thickness of ~ 50 nm grown by MOCVD

on free standing halide vapor phase epitaxy (HVPE) GaN, we showed (by measuring the lattice spacing along the c-axis) that the InGaN layer was divided at least into two sublayers with the In content increased toward the surface, in good agreement with the results reported by others.[30] This compositional stratification was also confirmed by energy dispersive x-ray spectroscopy (EDXS), which showed a 10 nm thick InGaN layer adjacent to GaN with 4.4% ± 0.5% In, followed by a top 25 nm thick layer with 10.3% ± 0.5% In. Such a phenomenon of higher In concentration toward the sample surface was observed by other researchers,[31] and it was sometimes referred to as a "pulling effect."[32] These experimental observations were also supported by theoretical considerations.[33]

In order to further verify our TEM and x-ray results, RBS studies were performed on the same samples (x = 0.1 and layer thickness in the range of 100–1000 nm). RBS provided composition profiles of InGaN layers as a function of layer thickness. The results of the RBS measured layer profiles of InGaN with various thicknesses are shown in Table I. Only the thinnest samples with flat surfaces showed almost identical thickness (exactly 69 ∼ 70 nm and 63 nm, respectively, from TEM and RBS) and an In composition of 7.3% by x-ray studies and 7% by RBS. This difference in the layer thickness observed across different techniques was most likely caused by differences in the surface roughness of the samples and the specific areas where the measurements, such as TEM, were taken. The experimental and calculated RBS spectra are identical for the thin layers (see Fig. 4 in Ref. 27) For the thicker layers, it was impossible to fit the experimental RBS spectra by assuming a single layer with uniform composition. Table I shows the schematic layer structures for InGaN samples with different thicknesses obtained by the best fit of the RBS data. The agreement was obtained only when the relaxed parts of the layers were sequestrated into sub-layers with different In contents (Table I). These results suggest that a high density of structural defects and their different atomic arrangement may lead to the local composition change. Since the thicker layers have more structural defects, they also have more nonuniform composition along the growth direction.

The layer stratification in thick InGaN layers was also investigated by high magnification TEM micrograph (HREM). Already for the 400 nm thick samples, long stacking faults appear in the strained areas and their density is higher in the thicker samples [Figs. 4(a)–4(c)]. This is in agreement with the diffused InGaN node observed in the RMS [Fig. 3(b)]. In these thick InGaN layers, HREM reveals that high density of dislocations and long stacking faults connecting column-like structures separated by V-defects [Figs. 4(a) and 4(c)] are formed. The arms of these V-shaped defects are on {10$\bar{1}$1} planes, the same as those previously observed in GaN.[34] The surface of these layers became very corrugated with saw-like shape [Figs. 4(a)–4(c)].

There are areas (marked by rectangular white brackets in all Fig. 4) where closely arranged stacking faults forming small "domains" are present. High magnification TEM micrograph (HREM) from part of such a domain is shown in [Fig. 5(a)]. Z-contrast microscopy reveals the presence of basal stacking faults ABABCBCB called I_1 and ABABCACA called I_2 (each capital layer stands for a double layer like AaBb) separated by different numbers of cubic layers observed in these small domains. The number of

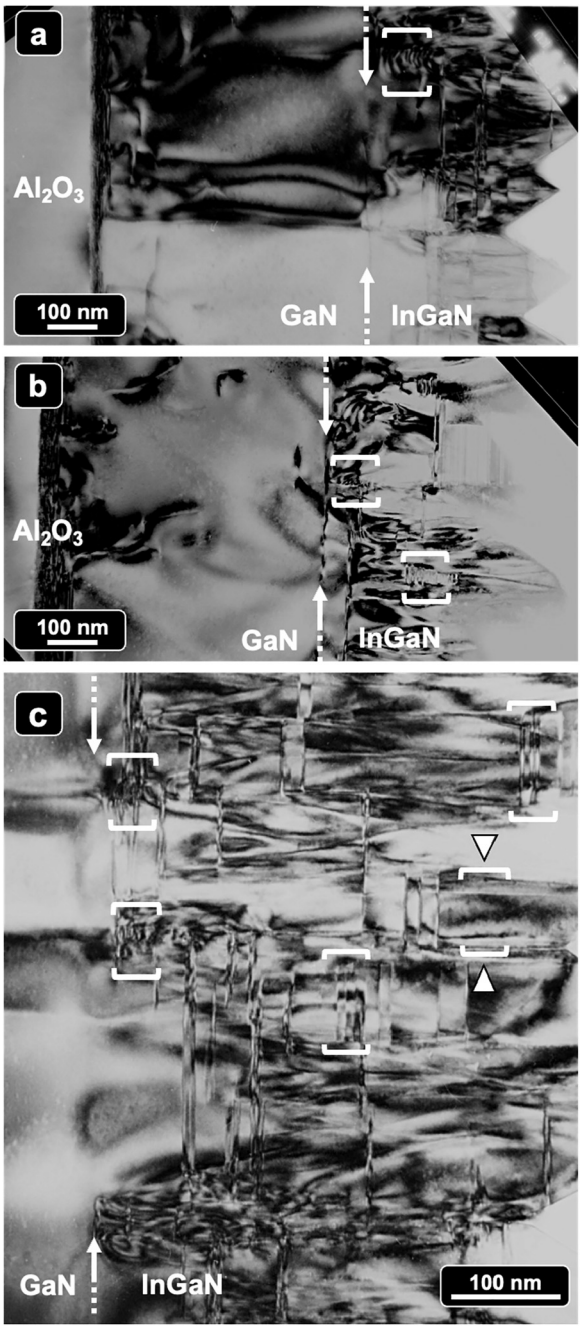

FIG. 4. (a) The micrograph from the $In_xGa_{1-x}N$ layer with nominal 10% In and the nominal thickness of t ∼ 500 nm, (b) t ∼ 750 nm, and (c) ∼1000 nm. Note surface corrugation with increased sample thickness, "saw-like" features (V), formation of long stacking faults, and small domains with closely distributed stacking faults marked by rectangular white brackets. The magnified image from the part of the bracket indicated by the arrow is shown in Fig. 6. The white arrows with dotted lines indicate the interfaces with GaN. Note a columnar growth in (c) and long stacking faults connecting these columns as well as large areas free of structural defects close to the interface with GaN.

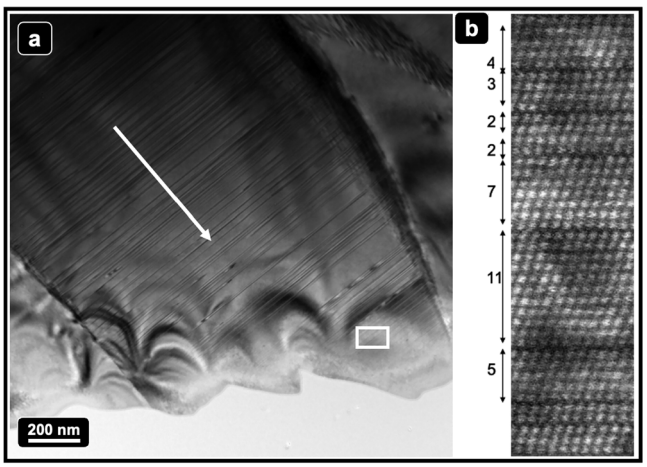

FIG. 5. (a) Densely distributed stacking faults within one grain. The area close to the sample surface is shown. The arrow indicates the growth direction; (b) high-resolution Z-contrast micrograph from the small area outlined by a white bracket in (a) with stacking faults intercepted by different sequences (marked by numbers) of cubic layers.

cubic layers [marked by numbers in Fig. 5(b)] can increase in the upper parts of the domains or a whole grain can stay cubic in the areas close to the surface. Therefore, the layer surface structurally is not uniform, with a mixture of cubic and hexagonal InN and different number of cubic materials between stacking faults.

Our XRD studies further corroborate the layer stratification in thick InGaN layers observed by TEM, RSM, and RBS. Figure 6(a) shows the 2Q/w scans of nominally 10% In InGaN layers with different layer thicknesses. The narrow peak at 2Q = 34.55° and the broad peak from InGaN at 2Q ~ 33.9°–34.2° correspond to the 0002 diffraction from GaN and InGaN, respectively. The InGaN peak starts to split into at least two peaks for layers thicker than 200 nm. This clearly suggests layer stratification with different compositions, confirming the results from RBS,[27] HREM, and EDXS[29] measurements.

B. Optical results

Photoluminescence studies were applied to InGaN samples with different thicknesses and nominal 10% In contents, in order to see how the presence of different structural defects and their different arrangement within the samples influences their PL emission. The PL spectra from these samples are shown in [Fig. 6(b)], and their luminescence peaks are distributed from 405 to 490 nm (corresponding to 4.06 to 2.53 eV) for samples with the nominal thickness from 100 to 1000 nm. The In fraction corresponding to the emission peak position from the band-edge luminescence is marked in this figure. Only for the thinnest sample (~100 nm—the micrograph shown in Fig. 2), the PL peak is reasonably narrow and at the position corresponding to 10% In. For the sample with the nominal of 250 nm, the PL peak becomes slightly broader and red shifted, indicating a substantial increase in the In content to 17% [the micrograph shown in Fig. 4(a)]. With a further increase in the layer thickness to 500 nm (nominal), the PL peak red shifts even more to the position corresponding to ~19% In. In addition, a second peak appears at longer wavelength, which suggests a phase with even larger In content of (23%). The TEM micrograph of this sample shows a corrugated surface (saw-like) with V-defects and domains with closely arranged stacking faults. For the sample with even higher thickness (nominally 750 nm), the PL peak position is very broad centered at ~ 440 nm, which is blue shifted compared

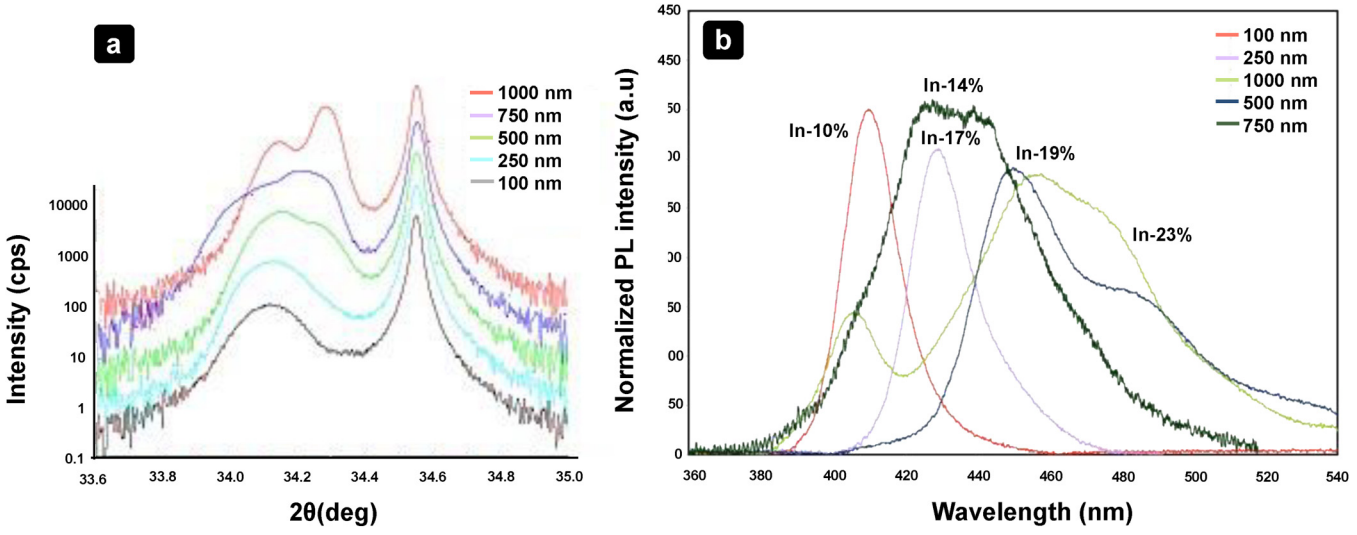

FIG. 6. (a) The results of 2Q/w scans for samples with nominally 10% In and different sample thicknesses (shown nominal values); (b) normalized PI intensities from the same samples.

to the main peak from the 500 nm thick sample [the micrograph shown in Fig. 4(b)]. In this sample, very long stacking faults close to the interface with GaN are clearly visible from TEM. Finally, the highest thickness [nominal 1000 nm—the micrograph shown in Fig. 4(c)] exhibits the most interesting PL results, showing the appearance of three PL peaks, one with lower intensity at the position comparable (but slightly blue shifted) to the peak from the thinnest sample. The position of this peak would indicate an In concentration lower than 10% In. Furthermore, two additional peaks that would indicate very high In concentration 19% and 23% are also prominent. In droplets were not observed in these samples, and other measurements (TEM, XRD, and RBS) showed a much smaller In content in this sample. These multi-peaks cannot be explained by an In increase close to the sample surface. It is clear evidence that these luminescence peaks arise from defects observed in these samples and the atomic arrangement as observed by TEM.

One also needs to notice that in the thickest sample in this study (1000 nm), an additional diffraction peak was also observed in the 2Q/w XRD scan [Fig. 6(a)]. TEM studies reveal columns with high density of defects starting almost at the interface with GaN. The long stacking faults are connecting these columns. It was noticed that the areas close to the interface with GaN below these stacking faults are practically defect free (see the interface area—central part in Fig. 4(c)), almost like in the samples with the smallest thickness. The defect-free area may give rise to the PL peak, almost at the same position as in the thinnest sample. However, next to these defect-free areas, the column-like features with high density of defects (mainly densely distributed dislocations) appear already at the interface with GaN and propagate to the sample surface. At the surface in these saw-like structures, the "chimneys" with dislocations are surrounded by domains with high density of stacking faults (like these shown in Fig. 5) often with large cubic areas between them or polytype-like structures. The surface morphology and its roughness are very complex.

PL peaks from the samples with thickness > 200 nm with the wavelength from 405 to ~430 nm appear to be consistent with the layer sequestration with different In contents, as suggested by RBS and RSM studies. However, all peaks with higher wavelengths most probably are originating from the structural defects with different atomic arrangements. These results were confirmed by CL studies on cross section samples (prepared in a similar way as for TEM), where different peaks appeared depending on the electron beam positions in different areas of the same sample (e.g., areas with different structural defects). These studies confirm that the appearance of multiple CL peaks (and PL peaks) is not only related to the compositional change but also influenced by structural defects present in those samples. Red shifts of the PL peak position consistent with our results were observed by other authors[35] in the samples with high defect density especially V-defects and trench defects.

III. COMPOSITIONAL MODULATION

InGaN used in different devices in most cases are grown directly either on GaN or AlN buffer layers on sapphire or SiC substrates. Such growth always leads to the strain in the layer due to lattice mismatch. As could be seen from the above results, even

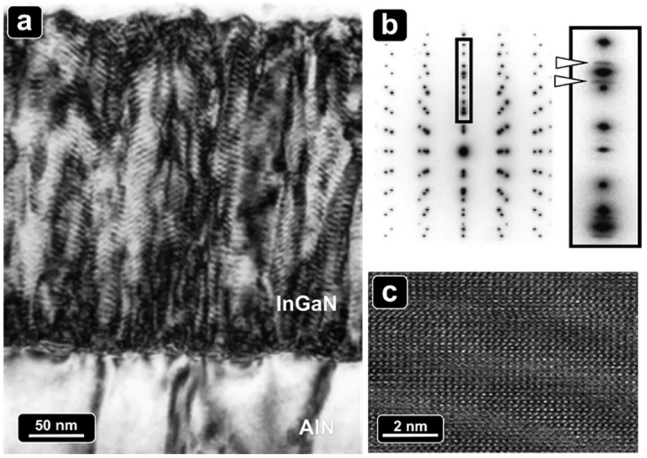

FIG. 7. (a) TEM micrograph showing compositional modulation in the $In_xGa_{1-x}N$ (x = 0.5); (b) diffraction pattern from the same sample (x = 0.5) in [1120] projection with arc reflection showing modulation on particular planes. In order to better see these arcs (marked by arrows), the enlarged part of the diffraction pattern is presented on the side. (c) Z-contrast micrograph showing the arrangement of the modulation fringes. White dots indicate heavier atoms (In).

with the low In content 10%, only a thin (~70 nm) InGaN layer close to the GaN (AlN) will be strained and with an increase in the sample thickness relaxation of the strain occurs and structural defects are formed. It turned out that strain relaxation can be realized in different ways. Compositional stratification as we have discussed earlier is one commonly observed strain relaxation mechanism. Other common mechanisms include the formation of planar defects (stacking faults), which leads to polytype-like structures or the composition modulation of InGaN layers. Previous works[36–38] reported that $In_xGa_{1-x}N$ layers with the high x ($0.45 < x < 0.78$) grown by MOCVD with AlN or GaN buffer layers showed light and dark contrast fringes [Fig. 7(a)] with the shallow "W" profile. This was observed by HRTEM in cross-sectional samples in two perpendicular zone axes, [1100] and [1120]. Electron diffractions in these both zone axis show the formation of extra spots in the form of small arcs [marked by arrows in Fig. 7(b) and an enlargement on the side]. High-resolution Z-contrast microscopy [Fig. 7(c)] and energy dispersive x ray (EDX)[36–38] showed substantial changes in the modulation amplitude of these black/white fringes.

This suggests some atomic segregation of higher atomic number elements, such as In. In these samples with high In content, the columnar growth was observed [Fig. 7(a)], with columns separated by dislocations (or low angle grain boundaries). The arrangement of these black/white fringes remains the same within one grain (the fringes are parallel to each other), but their position slightly changes from grain to grain (column to column). This can explain the presence of small arcs in the diffraction patterns (instead of the well-defined dots) and can suggest that In segregation somehow occurs possibly on the particular crystallographic planes. The spread angle of these arcs on the diffraction pattern was measured to be about ±30° with respect to the c-axis

[Fig. 7(b)], consistent with the inclination of the fringe position ±60° in Z-contrast TEM images [Fig. 7(a)]. Since these tweed-like fringes can be observed in two perpendicular orientations—[1100] and [1120] arranged almost at the same angle to the c-axis, this would suggest that the segregation plane must have a sixfold symmetry. Analyses of the contrast on white fringes on Z-contrast micrographs reveal some local segregation of heavier atoms (In) on {10$\bar{1}$1} planes [Fig. 7(c)], which was theoretically predicted by Northrup and Neugebauer.[39] Benamara[40] observed pits (V-defects) in AlGaN due to some ordering of alternating GaN and AlN layers on the step edges on {10$\bar{1}$1} pit facets. These planes are polar, and they are inclined ∼62° to the c-axis.

This composition modulation in the $In_xGa_{1-x}N$ samples with high x was also confirmed by the XRD results,[34–35] which showed a modulation period Δ = 47 Å in the sample with x = 0.5 and Δ = 58 Å in the sample with x = 0.78 (45 and 65 Å determined by TEM). The difference in the results obtained by the two different techniques can be justified by the difference in the studied sample areas. The compositional ordering on particular crystallographic planes was observed by other authors in such alloys as GaInP,[41] but in most cases, this was assigned to spinodal decomposition.[42–44] However, it appears that in our case of InGaN, this might be driven by a very rough interface between AlN and InGaN and a large lattice mismatch of about 14%. For the growth of $In_xGa_{1-x}N$ with a lower x = 0.34 on GaN where there is only 2% mismatch and more planar interface, such modulation was not observed.

The observed In segregation on {10$\bar{1}$1} planes[36] may also lead to the bending of the c-planes, and, therefore, these black/white fringes can deviate from other planes, also contributing to arc formation in the diffraction patterns. There are reports that compositional modulation developed on the surface can result in the growth of columnar structures with nodules oriented in specific crystallographic directions.[45] This columnar growth was also observed in our samples. EDX studies of these black/white fringes showed the alternating increase (decrease) in the In-K_a (Ga-K_a) peak intensity, and this reverses in the neighboring fringe.[36] The average estimated composition on the black fringe was ∼40% In and ∼60% of Ga. Considering the average composition of the layers, it can be calculated that alternate layers of GaN(+In)/InN(+Ga) were formed with the separation of 47 Å in samples with x = 0.5 and 58 Å in samples with higher In concentration (x = 0.78).

The PL studies on In-rich InGaN samples (e.g., x = 0.5) with compositional modulation showed that the luminescence peak was broader and was ∼0.5 eV redshifted from the absorption edge ("Stoke's shift"). This was a sample with a columnar growth and the highest density of dislocation among all three samples. Therefore, it is assumed that the modulation in the sample with x = 0.5 was strain driven and the corrugated surface of the AlN buffer layer initiated this modulation.

IV. QUANTUM WELLS AND V-DEFECTS

A. Inhomogeneity of QWs

$In_xGa_{1-x}N$/GaN quantum wells (QWs) are a key component in high performance opto-electronic devices. Therefore, in this section, several issues present in the samples with InGaN QWs will be considered. TEM studies were applied to such samples to find out about the compositional homogeneity of QWs and determine what were the most typical defects in such samples. Quantitative high-resolution transmission electron microscopy was used to study the distribution of indium atoms in $In_xGa_{1-x}N$ layers and QWs.[46–47] Layers with x = 0.6 and x = 0.7 have been studied. The results show the formation of In-rich clusters that are distributed in stripes with 2–4 nm periodicity and amplitude of Δx = 0.1 and Δx = 0.15 in the respective samples. These reports[46–47] indicated the similarity of the fluctuation amplitude and the formation of "dot-like" features in $InxGa_{1-x}N$ QWs and suggested that the spinodal decomposition occurred in both: layers and QWs. The report on the investigation on quantum wells[47] also showed an asymmetric In distribution across the well with respect to the growth direction. The broadening at the lower interface was observed at an extension of about 1 nm but more than 2 nm at the upper interface. These findings were also confirmed by Benamara et al.[48] who studied samples with 5 period $In_{0.3}Ga_{0.97}N/In_{0.13}Ga_{0.87}N/ In_{0.3}Ga_{0.97}N$ QWs and also 20 period $GaN/In_{0.2}Ga_{0.8}N$/GaN QWs. In both cases, the wells were 2.5 nm thick separated by 50 nm thick barriers. Quantitative HREM was used to map the strain profile across the well. Both "a" and "c" parameters were measured. They showed that in the sample with five QWs, the QWs were pseudomorphic and were under biaxial compression stress. The indium content in the QWs showed un-uniformity within the well. The upper interface was much broader compared to the lower interface, similar to the results shown in Ref. 47. The well composition was measured as 15% similar to the intended 13%. The In redistribution within the wells in the form of quantum dots was more apparent in the well with 20% In and dot size about 30 Å with a separation of 40 Å. The wells with higher In content were highly strained most probably due to the large difference in the lattice parameter between the well and barrier. A high density of dislocations and dislocation loops was observed at the upper interface but not at the lower interface. Therefore, the chemical mapping could not be obtained in these samples.

B. Surface roughness, V-defects in QWs

The new unpublished data of samples with different numbers (5 and 20) of $GaN/InxGa_{1-x}N$/GaN QWs but the same In content in the wells (x = 0.1) in both samples showed different surface roughness (rms) values as measured by atomic force microscopy (AFM). The surface roughness for samples with 5 QWs with measurements on $40 \times 40\,\mu m^2$ area was 2 nm, on $10 \times 10\,\mu m^2$ was 1.7 nm, and on $2 \times 2\,\mu m^2$ was 1.0 nm, but on the samples with 20 QWs measured on the same areas yielded roughness values of 5, 4.8, and 3.7 nm, respectively. These results show that the surface roughness is affected by the number of QW periods and it increases more than two times with an increase in the number of QWs. This could be explained by the presence of V-defects in these QWs layers. V-defects were formed in both types of samples but with much lower density in samples with 5 OWs.

Cross-sectional TEM studies show that these defects in most cases start to appear in the second QW (Fig. 8), but occasionally, they can be formed (not shown here) at the first QW, at the position where the substrate dislocations propagated through the well. With an increase in the number of QWs, new V-defects would be

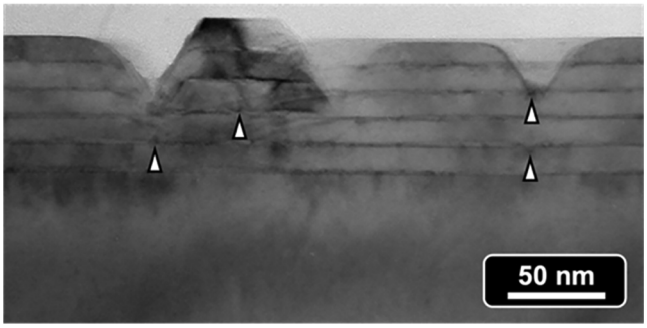

FIG. 8. Formation of V-defects in samples with 5 QWs. The arrows show the apexes of these defects.

formed on the lower interfaces with GaN barriers (even at dislocation free areas). Such defects would propagate to the sample surface. Therefore, in the samples with 20 QWs, the number of V-defects increased and, consequently, the surface roughness increased (no substantial change from area to area). It could be seen that in the sample with 20 QWs, the roughness was larger but changed from 5 to 3.7 nm (1.35 times) when compared to the largest measured areas with the smallest, whereas for samples with 5 QWs, it changed two times. This is because the distance between V-defects is larger in the latest samples.

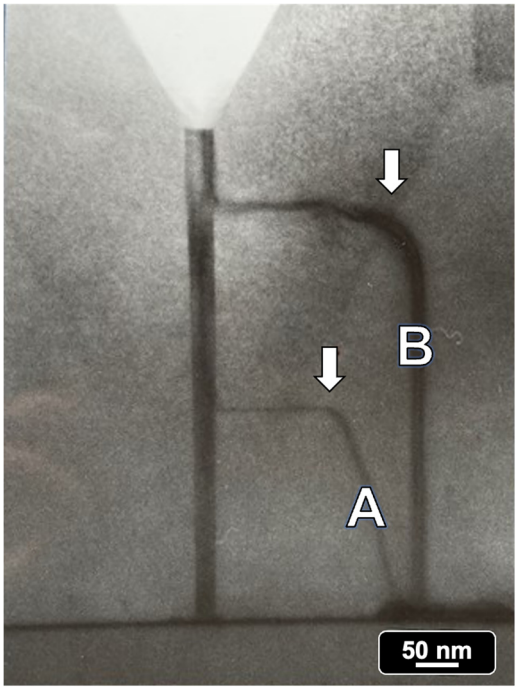

FIG. 9. A V-defect formed at the inversion domain (the center) at the interface and two dislocations of different types (A and B) formed far from the apex of V-defects. Note the different layer contrast (shades) indicating the growth along the c-axis (the right-hand side) and shaded-growth on the sidewalls on the V-defect. The white arrows show the areas of dislocation bending and attraction to the surface of the V-defect and further propagation to the inversion domain. First, dislocation A is attracted and with further growth B dislocation is attracted. Note the bending of dislocation at the same distance from the walls of the V-defect.

V-defects are inverted pyramids with six walls formed on {10$\bar{1}$1} polar planes. When seen in the cross section, projected planes form V-arms with 56° angle between them (Fig. 9). The growth on these planes is different than on basic polar c-planes and usually is the slowest. These are the same types of defects as observed in GaN.[34, 49–50] The difference in the growth rate in GaN on (0001) and (000$\bar{1}$) planes is well accepted due to different surface terminations—Ga and N. It is also known that the slower the growth rate, the more the impurities will be introduced. Therefore, as soon as any step or cumulation of "foreign atoms" (in the form of dopant or impurities) occurs, such a V-defect can be formed and simultaneous growth on c-plane and {10$\bar{1}$1} planes will take place.

It was shown by Liliental-Weber[34, 50] that in GaN layers grown on dislocation free bulk GaN, these two different growth fronts occurred and the layer thickness along the c-axis and perpendicular to the {10$\bar{1}$1} planes forming V-defect are very different. This observation was possible only because of the different contrast occurred on TEM micrographs for the layers grown along both directions. Responsibility for this difference in micrograph contrast most probably was different impurity cumulation on the slow growth rate {10$\bar{1}$1} planes, as usually observed on the −c (N-polarity) and +c (Ga polarity) growth of GaN.

Two different growth modes are not desirable for the growth of $InxGa_{1-x}N$ QWs. As shown by Wu[51] and Liliental-Weber,[50] much thinner QWs than these grown intentionally along the c-axis are formed on the {10$\bar{1}$1} sidewalls of V-defects. The presence of two different thicknesses of QWs will influence optical properties of desired devices. Therefore, research is ongoing on the elimination of V-defects.

V. DISCUSSIONS

The question remains to understand why V-defects are formed and where they originate. In many scientific papers,[30–31, 51–54] the authors connected the appearance of V-defects with the presence of dislocations. Indeed, the strain field around dislocations can cause the cumulation of dopants or impurities around the dislocations and dislocations will be always the first areas where such defects could be found (Ref. 34, Fig. 1). The V-defects in InGaN are the same types of defects as observed in GaN,[34, 49, 50] and they also appear when layers are grown on dislocation free substrates [Ref. 34, Figs. 2(b) and 3; Ref. 50, Fig. 5]. Previously, we showed [Ref. 49, Fig. 2(a) and Ref. 34, Fig. 2(c)] seven V-defects at the InGaN/AlGaN QW with only two dislocations at which V-defects occurred but the remaining five V-defects were formed between these dislocations. Theoretical calculations also do not give a full picture to explain the reason for their formation. Northrup *et al.* showed the segregation of In on {10$\bar{1}$1} facets that are forming the arms of V-defects[39] around the screw dislocations, but Shiojin *et al.*[52]

showed experimental observation that most of V-defects are formed around edge dislocations.

In the work of Liliental-Weber *et al.*,[34,50] it was shown that observing V-defects at dislocations does not mean that they originated from them. Figure 9 shows the V-defect originally formed close to the interface of GaN grown on the bulk GaN substrate, on the top of the inversion domain and two different types of dislocations (A and B) formed far from this V-defect. When growth proceeded along both the c-direction and newly formed walls of the V-defect (on inclined {10$\bar{1}$1} plane), lower dislocation A (located closer to V wall) was attracted to the free surface of this V-defect, by the so called "image force,"[55–56] at a required proper distance from the surface (see dislocation A bending marked by the arrow). When the growth continued and sidewalls of the V-defect were at the required distance from dislocation B, the same attraction force worked also for this dislocation. Both dislocations were attracted to the sidewall of the V-defect. One needs to notice that both dislocations bend at the same distance from the {10$\bar{1}$1} surface of the V-defect. As stated by Shima *et al.*[54] the magnitude of the attraction force "depends only on the distance *d* from the surface" and is "inversely proportional to this distance." If this sample area would be observed in plan-view, it would show the V-defect at dislocations! Such dislocations propagate further to the sample surface as the so called 'surface dislocations" originally described by Petroff[57] in different materials. Any dislocation formed in the material must propagate to the surface influencing the surface morphology with the exception of dislocation loops that can be imbedded within the material. Many V-defects found at dislocations do not necessary originate at them, and many of these V-defects are formed at dislocation free areas. Therefore, new explanations and new models that would consider a broader approach for V-defect formation require further work.

Many studies showed that definitely, layers with the smallest number of dislocations will show better optical performance; therefore, several methods to minimize dislocation density were developed such as strain-layer superlattices that help bending the dislocations from the active areas of the devices. It was shown[49] that in GaN, the number of V-defects increased when the O concentration increased and clearly showed that with intentionally introduced dopants, the number of V-defects drastically increased and their density can be governed by the growth condition such as temperature.[58] By changing the growth temperature, different In concentrations can be introduced[58] and, therefore, also different strains in the layers due to the difference in the atom size of Ga and In.

VI. CONCLUSION

Different works that were reviewed here showed that In is not uniformly distributed in InGaN layers or quantum wells. Indium sequestrations in the layers and also non-uniformities in layers and QWs on the atomic level are present. An increase in layer thickness or In content leads to various structural defects. These include V-defects and a transformation to a cubic structure characterized by a high density of stacking faults, resulting in the formation of polytype-like structures. Such defects persist in samples grown currently. The observations and models indicating that dislocations are the sole source of V-defects are not entirely accurate. As demonstrated earlier (and shown above), dislocations can be drawn toward V-defects due to the formation of free surfaces on the prismatic {10$\bar{1}$1planes} with much slower growth rate than on c-planes. Dislocations do not constitute the sole cause of their formation. V-defects are also formed in dislocation free samples. The variance in the growth rate on different crystallographic planes, especially in alloys with large difference in the atomic size of their constituents, along with the influence of impurities and dopants governed by growth conditions such as temperature, undeniably contributes to the formation of V-defects. Detailed characterization using a variety of experimental techniques in close collaboration with crystal growers hopefully could lead to a decrease and eventually maybe to the total elimination in the density of these defects.

ACKNOWLEDGMENTS

This paper was devoted to the memory of Wladek Walukiewicz on the first anniversary of his death. The subject of this paper was chosen to remember our work in one group and Wladek's contribution to determine a low bandgap in InN and show the importance of this work for today's research. The experimental work was supported by the Director, Office of Science, Office of Basic Energy Sciences, Division of Materials Science and Engineering, of the U.S. Department of Energy under Contract No. DE-AC03-76SF00098. The authors wish to thank all colleagues who contributed to the original publications based on which this manuscript could be written: Dr. K. M. Yu the closest co-worker of Dr. Walukiewicz, Dr. J. Wu, J. W. Ager, all crystal growers Dr. S. M. Bedair, Dr. S. Nakamura, Dr. W. J. Schaff, Dr. M. C. Johnson, and Dr. E. D. Bourret-Courchesne as well as all colleagues who used a variety of experimental methods working together on the same samples to understand the InGaN microstructure and optical properties of these alloys: Dr. D. F. Ogletree, Dr. J. Z. Domagala, Dr. J. Bak-Misiuk, Dr. M. Hawkridge, Dr. J. Jasinski, Dr. M. Benamara, and Dr. C. Kisielowski.

AUTHOR DECLARATIONS

Conflict of Interest

The authors have no conflicts to disclose.

Author Contributions

Z. Liliental-Weber: Conceptualization (equal); Data curation (lead); Formal analysis (lead); Funding acquisition (lead); Validation (lead); Writing – original draft (lead); Writing – review & editing (lead). **Roberto dos Reis:** Data curation (equal); Writing – original draft (equal); Writing – review & editing (equal).

DATA AVAILABILITY

The data that support the findings of this study are available from the corresponding author upon reasonable request.

REFERENCES

[1]H. P. Maruska, D. A. Stevenson, and J. I. Pankove, Appl. Phys. Lett. **22**, 303 (1973).
[2]I. Akasaki, H. Amano, Y. Koide, K. Hiramatsu, and N. Sawaki, J. Crys. Growth **98**, 209 (1989).

[3]J. I. Pankove and H. Schade, Appl. Phys. Lett. **25**, 53–55 (1974).
[4]T. D. Moustakas, T. Lei, and R. J. Molnar, Phys. B **185**(1–4), 36–49 (1993).
[5]S. Nakamura, T. Mukai, and M. Senoh, Appl. Phys. Lett. **84**, 1687 (1994).
[6]I. Akasaki, S. Sota, H. Sakai, T. Tanaka, M. Koike, and H. Amano, Electron. Lett. **32**, 1105 (1996).
[7]S. Nakamura *et al.*, Jpn. J. Appl. Phys. **35**, L74 (1996).
[8]S. Nakamura *et al.*, Jpn. J. Appl. Phys. **35**, L217 (1996).
[9]T. A. Tansley and C. P. Foley, J. Appl. Phys. **59**, 3241 (1986).
[10]C. Stammpfl, C. G. Van de Walle, D. Vogel, P. Krueger, and J. Pollmann, Phys. Rev. **61**, R7846 (2000).
[11]D. C. Look, H. Lu, W. J. Schaff, J. Jasinski, and Z. Liliental-Weber, Appl. Phys. Lett. **80**, 258 (2002).
[12]J. Wu, W. Walukiewicz, S. X. Li, R. Armitage, J. C. Ho, E. R. Weber, E. E. Haller, A. Barcz, and R. Jakiela, Appl. Phys. Lett. **82**, 2805 (2004).
[13]H. Lu, W. J. Schaff, L. F. Eastman, and C. E. Stutz, Appl. Phys. Lett. **82**, 1736 (2003).
[14]T. Matsuoka, H. Tanaka, T Sasaki, and A. Katsui, in *Proceedings of the Sixteenth International Symposium on GaAs and Related Compounds, Karuizawa, Japan, 25–29 September 1989* (Institute of Physics, Bristol, 1990), p. 141.
[15]S. Yamaguchi, M. Kariya, S. Nitta, T. Takeuchi, C. Wetzel, H. Amano, and I. Akasaki, Appl. Phys. Lett. **76**, 876 (2000).
[16]V. Yu. Davydov, A. A. Klochikhin, R. P. Seisyan, V. V. Emtsev, S. V. Ivanov, F. Bechstedt, J. Furthmüller, H. Harima, A. V. Mudryi, J. Aderhold, O. Semchinova, and J. Graul, Phys. Status Solidi B **229**(3), r1–r3 (2002).
[17]C. H. Swartz, R. P. Tomkins, T. H. Myers, H. Lu, and W. J. Schaff, Phys. Status Solidi C **2**, 2250 (2005).
[18]P. Carrier and W. Su-Huai, J. Appl. Phys. **97**, 033707 (2005).
[19]J. Wu, W. Walukiewicz, K. M. Yu, J. W. Ager III, E. E. Haller, H. Lu, W. J. Schaff, Y. Saito, and Y. Nanishi, Appl. Phys. Lett. **80**, 3967 (2002).
[20]Y. Nanishi, Y. Saito, and T. Yamaguchi, Jpn. J. Appl. Phys. **42**, 2549 (2003).
[21]W. Walukiewicz, S. X. Li, J. Wu, K. M. Yu, J. W. Ager III, E. E. Haller, H. Lau, and W. Schaff, J. Cryst. Growth **269**(1), 119–127 (2004).
[22]W. Walukiewicz, J. W. Ager III, K. M. Yu, Z. Liliental-Weber, J. Wu, S. X. Li, R. E. Jones, and J. D. Denlinger, J. Phys. D: Appl. Phys **39**, R83–R99 (2006).
[23]F. Bechstedt, J. Furthmuuller, M. Ferhard, L. K. Teles, L. M. R. Scolfaro, J. R. Leite, V. Y. Davudov, O. Ambacher, and R. Goldhahn, Phys. Status Solidi A **195**, 628–633 (2003).
[24]P. Carrier and S.-H. Wei, J. Appl. Phys. **97**, 033707 (2005).
[25]Z. Liliental-Weber, M. Benamara, J. Washburn, J. Z. Domagala, J. Bak-Misiuk, E. I. Piner, J. C. Roberts, and S. M. Bedair, J. Electron. Mat. **30**(4), 439 (2001).
[26]Z. Liliental-Weber, K. M. Yu, M. Hawkridge, S. Bedair, A. E. Berman, A. Emara, J. Domagala, and J. Bak-Misiuk, Phys. Status Solidi C **6**(S2), S433–S436 (2009).
[27]Z. Liliental-Weber, K. M. Yu, M. Hawkridge, S. M. Bedair, A. E. Berman, A. Emara, D. R. Khanal, J. Wu, J. Z. Domagala, and J. Bak-Misiuk, Phys. Status Solidi C **6**(12), 2626–2631 (2009).
[28]Z. Liliental-Weber, D. F. Ogletree, K. M. Yu, M. Hawkridge, J. Z. Domagala, J. Bak-Misiuk, A. E. Berman, E. Emara, and S. Bedair, Phys. Status Solidi C **8**(7–8), 2248 (2011).
[29]J. Jasinski, Z. Liliental-Weber, D. Huang, M. A. Reshchikov, F. Yun, H. Morkoç, C. Sone, S. S. Park, and K. Y. Lee, MRS Online Proc. Libr. **722**, 31 (2002).
[30]L. Goregos, O. Ambacher, M. Stutzmann, C. Miskys, F. Scholz, and J. Off, Appl. Phys. Lett. **76**, 577 (2000).
[31]T. B. Eldred, M. Abdelhamid, J. G. Reynolds, N. A. El-Masry, J. M. LeBeau, and S. M. Bedair, Apply.Phys. Lett. **116**, 102104 (2020).
[32]K. Hiramatsu, Y. Kawaguchi, M. Shimizu, N. Sawaki, T. Zheleva, R. F. Davis, H. Tsuda, M. Taki, N. Kuwano, and K. Oki, MRS Int. J. Nitride Semicond. Res. **2**, 6 (1997).
[33]A. I. Duff, L. Lymperakis, and J. Neugebauer, Phys. Rev B **89**, 085307 (2014).
[34]Z. Liliental-Weber, Y. Chen, S. Ruvimov, and J. Washburn, Phys. Rev. Lett. **79**(15), 2835 (1997).
[35]K. Prabakaran, R. Raju, P. Arivazhagan, M. Jayasathi, S. Sanjay, S. Surender, S. Pradeep, M. Balaji, and K. Baskar, J. Alloys Compd. **811**, 151803 (2019).
[36]Z. Liliental-Weber, D. N. Zakharov, K. M. Yu, J. W. Ager III, W. Walukiewicz, E. E. Haller, H. Lu, and W. W. J. Schaff, J. Electron Microsc. **54**(3), 243–250 (2005).
[37]Z. Liliental-Weber, D. N. Zakharov, K. M. Yu, J. W. Ager III, W. Walukiewicz, E. E. Haller, H. Lu, and W. W. J. Schaff, Mater. Res. Symp. Proc **831**, E.11.19 (2004).
[38]Z. Liliental-Weber, D. N. Zakharov, K. M. Yu, J. W. Ager III, W. Walukiewicz, E. E. Haller, H. Lu, and W. W. J. Schaff, Phys. B **376–377**, 468–472 (2006).
[39]J. E. Northrup, L. T. Romano, and J. Neugebauer, Appl. Phys. Letter. **74**, 2319 (1999).
[40]M. Benamara, L. Kriste, M. Albrecht, K. W. Benz, and H. P. Strunk, Appl. Phys. Lett **82**(4), 547–549 (2003).
[41]S. W. Jun, T. Y. Seong, and J. H. Lee, Appl. Phys. Lett. **68**, 3443 (1996).
[42]H. Ho and G. B. Stringfellow, Appl. Phys. Lett. **69**, 2701 (1996).
[43]O. Ueda, S. Isozumi, and S. Komiya, Jpn. J. Appl. Phys. **23**, L241 (1984).
[44]A. Zunger and S. Mahajan, in *Handbook on Semiconductors*, edited by S. Mahajan (North Holland, Amsterdam, 1994), Vol. 3, pp. 1399–1514.
[45]S. N. G. Chu, S. Nakahara, K. E. Strege, and W. D. Johnston, Jr, J. Apply. Phys **57**, 4610 (1985).
[46]T. P. Bartel, P. Specht, J. C. Ho, and C. Kisielowski, Philos. Mag. **87**(13), 1983–1998 (2007).
[47]C. Kisielowski, Z. Liliental-Weber, and S. Nakamura, Jpn. J. Appl. Phys **36**, 6932 (1997).
[48]M. Benamara, Z. Liliental-Weber, W. Swider, J. Washburn, R. D. Dupuis, P. A. Grudowski, C. J. Eiting, J. W. Yang, and M. A. Khan, Mater. Res. Soc. Symp. Proc. **572**, 357 (1999).
[49]Z. Liliental-Weber, S. Ruvimov, W. Swider, Y. Kim, J. Washburn, S. Nakamura, R. S. Kern, Y. Chen, and J. W. Yang, Mater. Res. Soc. Proc. **482**, 375 (1998).
[50]Z. Liliental-Weber, J. Electron Microsc. **49**(2), 339–348 (2000).
[51]X. H. Wu, C. R. Elsass, A. Abare, M. Mack, D. Keller, P. M. Petroff, S. P. DenBaars, J. S. Speck, and S. J. Rosner, Appl. Phys. Lett. **72**, 692 (1998).
[52]M. Shiojin, C. C. Chuo, J. Y. Hsu, J. R. Yang, and H. Saijo, J. Appl. Phys. **99**, 073505 (2006).
[53]H.-L. Tsai, T.-Y. Wang, J.-R. Yang, C.-C. Chuo, J.-T. Hsu, Z.-C. Feng, and M. Shiojri, Mater. Trans. **48**(5), 894 (2007).
[54]H. Shima, Y. Umeno, and T. Sumigawa, R. Soc. Open Sci. **9**, 220151 (2022).
[55]B. Gurrutxaga-Lerma, D. S. Balint, D. Dini, and A. P. Sutton, Proc. R. Soc. A **471**, 0433 (2015).
[56]R. J. Asaro, J. Phys. F: Met. Phys. **5**, 2249 (1975).
[57]P. M. Petroff and R. J. Wilson, Phys. Rev. Lett. **51**, 199 (1983).
[58]M. C. Johnson, Z. Liliental-Weber, D. N. Zakharov, D. E. McCready, R. J. Jorgenson, J. Wu, W. Shan, and E. D. Bourret-Courshesne, J. Electron. Mater. **34**(5), 605 (2005).